COMPOSITE-TO-METAL TUBULAR LAP JOINT UNDER TORSIONAL LOADING

PETR BERNARDIN[1], FRANTISEK SEDLACEK[1], VACLAVA LASOVA[1], RADEK KOTTNER[2]

[1]University of West Bohemia in Pilsen, Faculty of Mechanical Engineering, RTI - Regional Technological Institute

[2]University of West Bohemia in Pilsen, Faculty of Applied Sciences, European Centre of Excellence, NTIS – New Technologies for Information Society

During the damage evolution of bonded joints, different modes of failure can be detected. These modes include pure modes (Mode I, Mode II, Mode III) or their combinations (Mixed-mode) according to the type and the direction of loading. Some scientifically validated test methods are commonly used to obtain the fracture toughness by loading under pure Mode I, Mode II and their Mixed-mode. Some test methods were established to obtain the fracture toughness by loading under pure Mode III, however further research is required. The aim of this work is to clarify the mode ratio of a tubular lap joint under torsional loading and then to propose a method to determine the cohesive and damage parameters of this joint.

The presumed mode of failure is Mode III, or Mixed-mode with a predominance of Mode III. Emphasis is placed on the widespread applicability of the obtained results for similar specimens loaded under similar modes.

KEYWORDS

Bonded joint, composite-to-metal, finite element, Scotch-Weld DP490, damage modelling, identification

1   INTRODUCTION

Composite materials are used for machine tools, the automotive industry, and aviation, where designs mostly consist of multiple parts and materials. This places high demands on the inter-part connections. There are several ways to create metal-to-composite connections. These are namely riveted joints, bolted joints, interference fit joints, taped riveted joints, integrated joints and bonded joints [Lašová 2013]. For riveted and bolted joints, the connecting elements are placed in the holes in the connected parts. These holes cause a concentration of the stress and significantly degrade the mechanical properties of composites. Interference fit joints are less suitable for metal-to composite connections because of the differences in thermal expansion, which can lead to an increase of the pressure or release of the interference fit joint [Bernardin 2016]. Therefore, composite-to-metal bonded joints seem to be a more appropriate option.
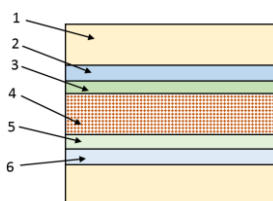

Figure 1. Sketch of specimen

The structure of the bonded joint is described in Fig 1, where (1) are adherends (bonded parts), (2) and (6) are adhesive zones, (3) and (5) are transitional cohesive zones, and (4) is the cohesive zone.

2   BONDED JOINT MODELLING OF TUBULAR LAP JOINT

The mechanical properties of the bonded joints (strength, stiffness) can be determined analytically. The finite element method (FEM) should be selected for predicting the mechanical properties of bonded joints for complex surfaces and it is also a good solution for describing damage initiation and damage evolution (until complete failure occurs).   There are many possibilities for modelling the adhesive layer and the adherends, differing in the level of idealisation and the size of the elements in the FEM model [Benzeggagh 1996, Camanho 2002]. Damage initiation can be evaluated using strength criteria, or by principles of fracture mechanics which also contain damage evolution. Energy principles based on fracture mechanics are used for thin adhesive layers, where the macroscopic properties (Young's modulus, Poisson's ratio) of the adhesive do not correspond to the real behaviour of the bonded joint [Simulia 2013]. This description is based on research [Griffith 1920, Irwin 1957, Inglis 1913], whose aim was to clarify elliptical crack propagation in structures.   One option for predicting damage initiation and damage evolution is a cohesive model corresponding with Griffith's energy principles [Griffith 1920]. Cohesive and damage parameters describe the process of failure in a cohesive model. These parameters are not usually provided by the adhesive manufacturer and strongly depend on the geometry and the type of loading of the bonded joint. During the damage evolution of the bonded joints, different modes (mechanisms) of failure can be detected. These are namely the pure modes (Mode I, Mode II, Mode III) or their combination (Mixed-mode) and are shown in Fig. 2.
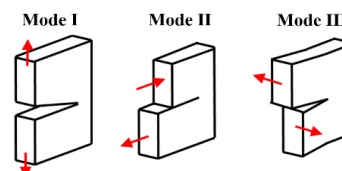

Figure 2. The failure modes

Each mode is described by its own cohesive and damage parameters. These are namely the critical strain energy release rate (SERR), which can be obtained for Mode I and II from experimental measurement according to ASTM [ASTM D5528-13 2014, ASTM D7905M-14 2013]. Several test methods were proposed to determine the critical energy release rate for Mode III [de Morais 2008, Liao 1996], for example, the Split Cantilever Beam test (SCB) [Davidson 2010], the Edge Crack Torsion test (ECT) [Ratcliffe 2004] or the Six Point Bending Plate test (SPBP) [Mehrabadi 2013]. Most of these contain a significant proportion of modes other than pure Mode III. There is no standardized testing method for testing components loaded by pure Mode III or by Mixed-mode containing Mode III. The authors of this research are focused in the long term on machine tool design and are also currently working on composite-to-metal drive shafts. Therefore, a tubular lap joint under torsional loading (TLTL) seemed to be a suitable choice. According to some sources [de Morais 2008, Liao 1996, Davidson 2010, Ratcliffe 2004, Mehrabadi 2013] these joints include a combination of modes (Mixed-mode), according to others [Li 2009] only pure Mode III is included. The aim of this work is to clarify the mode ratio of TLTL (pure Mode III or Mixed-mode with predominance of Mode III) and then propose a method to determine the

cohesive and damage parameters of this joint. The results should be useful for the subsequent design of the standardized method of joints under pure Mode III.

2.1 ANALYTICAL CALCULATION

The least time-consuming calculation method for predicting the TLTL is an analytical calculation [Gay 2003]. This method simplifies the real stress behaviour τ_{tr} (frictional shear stress component) to the average value τ_a. Fig. 3 shows the typical distribution of the τ_{tr} in the TLTL in the X direction (L is the length of the bonded joint) [Aimmanee 2018, Kaya 1999, Chen 1992].
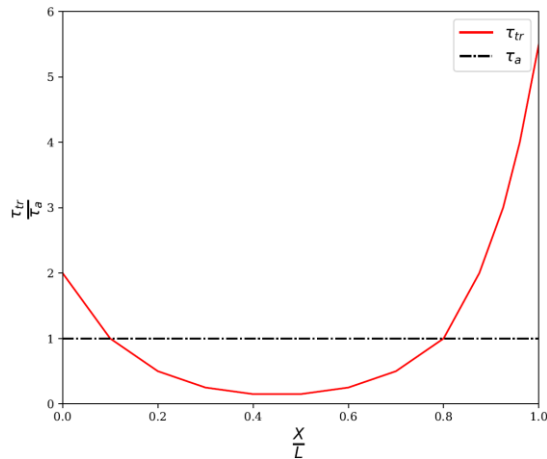

Figure 3. The typical stress distribution (τ) and the idealised stress distribution (τ_a) in TLTL
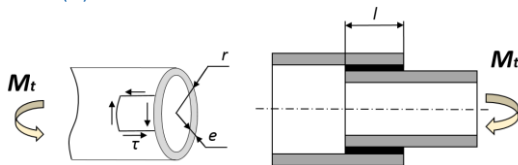

Figure 4. Sketch of TLTL analytical calculation

Fig. 4 shows all the parameters used for the analytical calculation according to Equation 1, which are described in Tab. 1.

$$\tau_{average} = \frac{M_t}{2 \cdot \pi \cdot r^2 \cdot l} \leq 0{,}2 \cdot \tau_{rupture}, \qquad (1)$$

Parameter	Description
r	Inner tube radius
$\tau_{rupture}$	Permissible shear stress
l	Length of the bonded surface
M_t	Applied torque

Table 1. All parameters used for analytical calculation

2.2 STRENGTH CRITERIA EVALUATED BY FEM

There are many possibilities for modelling the bonded joint, differing in the level of idealisation of the adherends and adhesive using FEM.
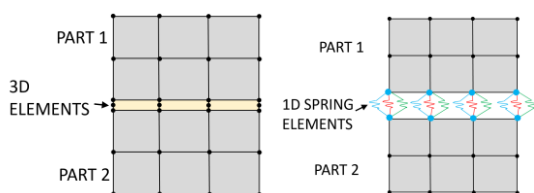

Figure 5. 3D elements (left) and 1D spring elements (right)

The adhesive layer can be idealized with 1D elements with defined or infinite stiffness or by 3D elements. This approach is described in Fig. 5. The maximum shear stress value is determined from 1D, or 3D elements in relation to the permissible shear stress (given by the manufacturer of the adhesive). The other possibility for bonded joint idealisation is Tahmasebi's model [Tahmasebi 1999], which combines the 3D solid elements with the 1D spring elements and 1D rigid elements. This model is described in Fig.6 and Fig.7.
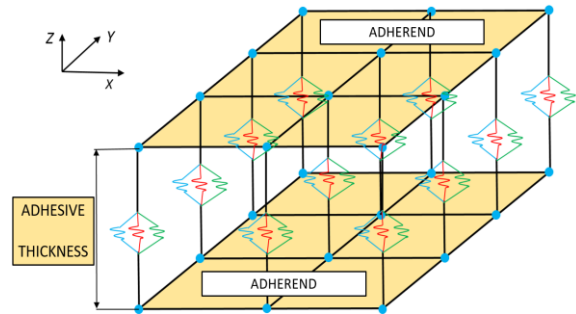

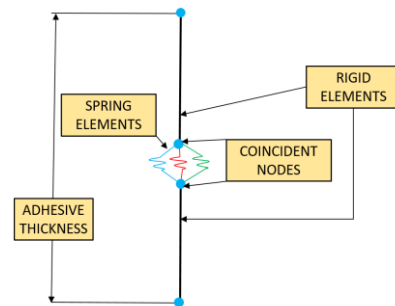**Figure 6.** Tahmasebi's model - 1D and 3D elements

Figure 7. Tahmasebi's model - 1D spring elements and 1D rigid elements

The maximum shear stress can be determined only in the middle of the adhesive layer (from the 1D spring elements), which is the major disadvantage of this model.

2.3 VIRTUAL CRACK CLOSURE TECHNIQUE

The virtual crack closure technique (VCCT) calculates the SERR, respecting that the energy needed to separate two surfaces is equal to the energy to close them [Gliszczynski 2019, Vigroux 2009, Krueger 2015]. This unique technique calculates iteratively the crack growth based on fracture mechanics using the nonlinear analysis with the help of convergence and stabilization algorithms. This method is applicable for bonded joints loaded by an arbitrary mode of failure (I, II, III or Mixed-mode), but the major disadvantage is the considerable time and computing demands.

2.4 EXTENDED FEM

The eXtended Finite Element Method (XFEM) also known as partition of unity method (PUM) or generalized FEM (GFEM), is a powerful and effective calculation technique for modelling failure problems without the requirement of remeshing. This method extends the conventional FEM and allows independent mesh crack modelling (see Fig. 8) [Belytschko 2009].
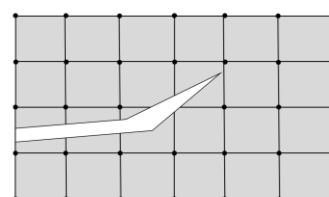

Figure 8. Crack modelling independent on mesh

The main field of application of this method is modelling of fracture, dislocations, grain boundaries, or phases interfaces.

2.5 COHESIVE ZONE MODEL

Nowadays, most FEM solvers use de-cohesion elements in different forms. For our specific purpose, we use cohesive surface based contact [Benzeggagh 1996, Camanho 2002] instead of the cohesive elements, which are now the two basic methods of cohesive modelling. These elements are based on the cohesive zone modelling approach (CZM) [Barenblatt 1962, Dudgale 1960]. This approach describes the bonded joint from the initial load until complete failure using the specific criteria. The cohesive behaviour of the joint is characterized by the cohesive stiffness criterion (k_n, k_s, k_t), where n, s, t are directions of the coordinate system. The damage initiation criterion and damage evolution law were used to simulate the loading and softening process of the bonded joints. The damage initiation criterion refers to the degradation of the cohesive stiffness of the layer of the adhesive. In our case, it was described by the quadratic stress, see Eq. 2.

$$\left\{\frac{\langle t_n \rangle}{t_n^o}\right\}^2 + \left\{\frac{t_s}{t_s^o}\right\}^2 + \left\{\frac{t_t}{t_t^o}\right\}^2 = 1 \qquad (2)$$

The denominator represents the maximum contact stress defined by the user (t_n^o, t_s^o, t_t^o) and the nominator represents traction stress. The t_n in Maxwell's bracket describes the different behaviour of the adhesive layer in positive and negative directions. The damage initiation (B point position) can be described (in three directions) by Eq. 3.

$$t = \begin{bmatrix} t_n \\ t_s \\ t_t \end{bmatrix} = \begin{bmatrix} k_n & 0 & 0 \\ 0 & k_s & 0 \\ 0 & 0 & k_t \end{bmatrix} \begin{bmatrix} \delta_n \\ \delta_s \\ \delta_t \end{bmatrix} = K\delta \qquad (3)$$

The pure modes are expected to be orthogonal in the loaded part. This should be reflected in the FEM model, where the directions of Mode I-III should correspond with the directions of n, s, t in the FEM analysis. The crack tip orientation should coincide with the direction of Mode III. This assumption is valid only in the case of direct crack propagation. The critical SERR (G_{nc}, G_{sc}, G_{tc}) describes the state of complete degradation of cohesive stiffness and is represented by the area under AB and BC curves in fig. 9.
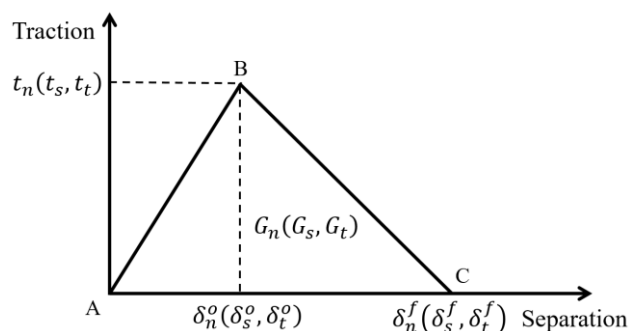

Figure 9. Linear damage parameters

The failure of the joint according to Mode I is performed using the Double Cantilever Beam (DCB) test method, the failure according to Mode II is performed using the End Notched Flexure (ENF) test method. The critical value of the G_{nc}, G_{sc} for Mode I and II (G_{Ic}, G_{IIc}) can be determined from experimental measurements according to the ASTM methods [ASTM D5528-13 2014, ASTM D7905M-14 2013] using Eq. 4 and Eq. 5 [Bernardin 2019, Ducept 2000, Zemčík 2008].

$$G_{Ic\ EXP} = \frac{3F_c\delta_c}{2b(a+\Delta)} \qquad (4)$$

$$G_{IIc\ EXP} = \frac{9a^2 F_c \delta_c}{2b(2L^3 + 3a^3)} , \qquad (5)$$

where F_c is the critical force related to the damage initiation, δ_c is the corresponding opening displacement, b is the width of the specimen, a is the initial opening length and L is the displacement between the position of the load and one support. As stated in the introduction, the determination of critical value G_{sc} for Mode III G_{IIIc} is not possible according to any standard method. Therefore, it is a task of this research to find one. Because the mode ratio in the tubular lap joint was unknown, the model was solved as loaded under Mixed-mode, defined by the 3D Power Law criterion [Reeder 2006] described in Eq. 6.

$$\left(\frac{G_I}{G_{Ic}}\right)^\alpha + \left(\frac{G_{II}}{G_{IIc}}\right)^\alpha + \left(\frac{G_{III}}{G_{IIIc}}\right)^\alpha = 1, \qquad (6)$$

where G is SERR, indexes I, II, III refer to the mode of failure, index c describes the critical value, index α is a dimensionless coefficient.

3 EXPERIMENT

Since there is no standard method for testing bonded joints loaded under pure Mode III, the shape of the specimen had to be designed as well as the whole testing method. The TLTL was chosen based on the motivation of the authors and previous research [Bernardin 2013]. The specimens consisted of a composite tube (Pos.2) and two steel rollers (Pos.1 and Pos.3). The dimensions and arrangement of all the parts are shown in Fig. 10 and Fig. 11.
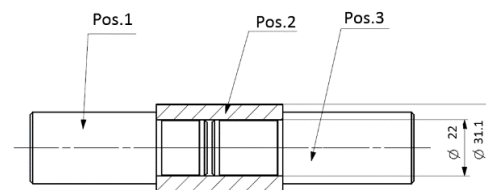

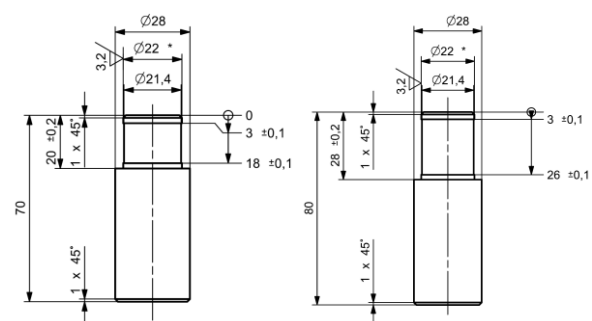**Figure 10**. Sketch of specimen

Figure 11. Sketches of specimen

The lengths of the bonded surfaces on both metal parts were different (15 mm and 23 mm), because of the controlled failure of the bonded joint with the shorter bonded surface. The influence of the various adhesive thicknesses was examined in depth. The strength of the bonded joint is not influenced by the change of the adhesive layer in the range of thickness from 0.05 mm to 0.4 mm [Sedláček 2005]. A detailed view of the adhesive layer is shown in Fig. 12, where L represents the length. T represents the thickness of the adhesive layer. The 0.3 mm value of thickness was chosen according to the adhesive manufacturer [3M 1996]. It corresponds with the previously recommended range.
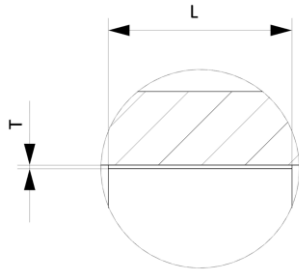
Figure 12. Sketch of specimen – Detailed view of the adhesive layer

Mechanical properties of the composite tube are shown in Tab. 2, where V_m is the matrix volume ratio, V_f is the fibre volume ratio, E is the Young's modulus and the 1, 2, 3 indexes refer to the material directions, v is Poisson's ratio, and G is the shear modulus.

Matrix		V_m
Epoxy resin		0.4
Fibre		V_f
34-700-12k		0.6
E_1[GPa]	E_2[GPa]	E_1[GPa]
142	5.7	142
v_{12} [-]	v_{23} [-]	v_{12} [-]
0.33	0.037	0.33
G_{12}[GPa]	G_{23}[GPa]	G_{12}[GPa]
2.65	1.1	2.65

Table 2. Material properties of composite tube

Fourteen specimens were experimentally tested. The adhesive Scotch-Weld DP490 was used, instead of Araldite or Spabond adhesives, for which the pull-up of the fibre was found [Bernardin 2013]. The specimens were torsionally loaded until failure at 21.2 °C, and at relative humidity 59%. The thicknesses and the fibre orientation of individual layers in the composite tube are shown in Tab. 3.

Layer number	Thickness [mm]	Fibre Orientation [°]
1	0.346	43.09
2	0.341	-43.98
3	0.968	0.00
4	0.324	47.1
5	0.320	-47.82
6	1.284	0.00
7	0.176	87.38
8	0.349	87.41
9	0.349	43.09

Table 3. Description of individual layers
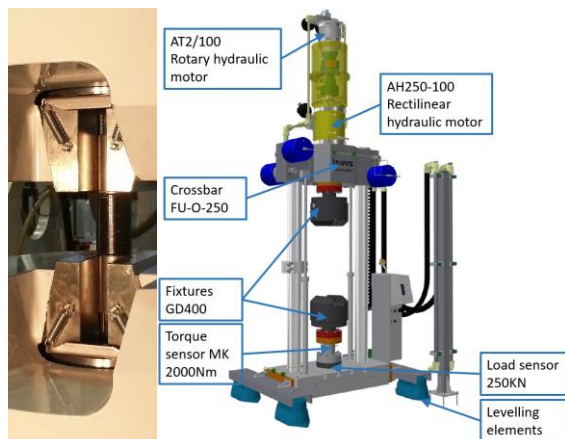

Figure 13. Specimen testing using FU-O machine (Torsional loading)

The universal testing machine FU-O and the clamped specimen are shown in Fig. 13 , and the measuring devices (motors, sensors, etc.) are labelled. All results obtained during measuring were processed using the TestControl software. The load was defined by angular velocity ω_y= 1°/min and the torque and the rotation were measured. The cohesive bonded failure (only in the adhesive layer) is expected during testing, but there was the concern that several external factors may affect the measuring results. These are namely the imperfect manual preparation of the bonded joint (variable circumferential thickness, air in the adhesive), imperfect manufacturing of the specimens (small roughness of the turned specimens), pull-up of the composite fibres, and the adhesive bonding failure (on the interface between the adhesive and adjacent part).

4 FINITE ELEMENT ANALYSIS

The model used for quasi-static FEM analysis was created in commercial software Abaqus/CAE 6.14. All parts were uniformly meshed using the eight-node linear brick elements (C3D8R). The partition cell feature was used for making the mesh more precise on the contact surfaces. The material and the boundary conditions were assigned to all three parts in the FEM model. The layer of the adhesive was idealised using surface-to-surface cohesive contact with defined mechanical properties.
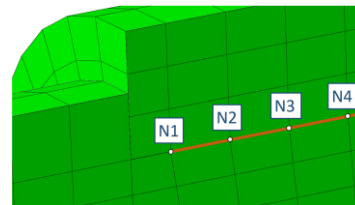

Figure 14. The cohesive surface-based contact for the adhesive layer idealisation

The cohesive surface based contact was applied on all coincident node pairs (N1-N4) in the layer of the adhesive with defined thickness 0.3 mm (respecting the real thickness of the adhesive). The meshed FEM model with specific boundary conditions (BC$_1$, BC$_2$) and a definition of the coordinate system (X, Y, Z) is shown in Fig. 15.
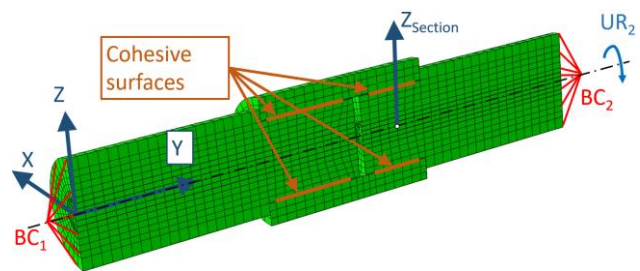

Figure 15. 3D meshed model with the boundary conditions and applied torque

All displacements and rotations (U_1, U_2, U_3, UR_1, UR_2, UR_3) of boundaries BC$_1$ and BC$_2$ were set to zero except the rotation UR_2 for boundary BC$_2$ which was set to 0.12 rad, which corresponds to the experiment.

5 IDENTIFICATION

The mechanical properties were identified using the gradient-based method optimisation in optiSLang software. k_n, k_s, k_t, t_n, t_s, t_t, G_{nc}, G_{sc}, G_{tc}, α were set as the input parameters. The initial values, lower and upper bounds are shown in Tab. 4.

Parameter	Initial value	Lower bound	Upper bound
k_n [GPa/m]	1000	20	5000
k_s [GPa/m]	1000	20	5000
k_t [GPa/m]	1000	20	5000
t_n [MPa]	15	0.5	200
t_s [MPa]	15	0.5	200
t_t [MPa]	15	0.5	200
G_{nc} [J/m^2]	2000	20	10000
G_{sc} [J/m^2]	2000	20	10000
G_{tc} [J/m^2]	2000	20	10000
α	1	0.2	5

Table 4. Input parameters of the gradient-based optimisation method

The gradient option algorithm is the NLPQLP (Nonlinear programming with non-monotone and distributed line search). Tab. 5 includes the gradient option parameters, which, together with input parameters, refer to the quality of the identification.

Gradient option	Type/Value
Algorithm	NLPQLP
Maximum iterations	300
Maximum function calls	300
Differentiation interval	central differences
Differentiation method	0.1
Maximum line-search function calls	50
Tolerance of QP solver	0.0
Accuracy of solution	1.0 E-9
Stack size merit function	10
Bound for increase of merit function	0.1 %

Table 5. The gradient option parameters

These parameters strongly influence the propagation of the objective function, which is marked r_g and describes the minimizing of the difference between the torque-rotation diagram obtained from FEM analysis and experimental testing. Eq. 7 describes this behaviour.

$$r_g = \sum_{i=0}^{n} \left(\frac{M_{FEA}^i - M_{exp.}^i}{\max_i (M_{exp.}^i)} \right)^2, \qquad (7)$$

where M_{FEA}^i is the torque obtained by the analysis and $M_{exp.}^i$ is the torque obtained by the experiment.

6 RESULTS AND DISCUSSION

To identify the cohesive and damage parameters of the TLTL, it was necessary to evaluate the results of the experiment and select a representative sample (representative behaviour).

Figure 16. Specimens with pull-up of the fibre (left) and specimens without the pull-up mechanism of failure (middle/right)

The ruptured specimens are shown in Fig. 6. The pull-up of the fibres occurred in three specimens. Two of them failed on the

longer side of the adhesive layer and one specimen on the shorter side. All these specimens were rejected from the identification process. A significant decrease of the transmitted torque was found in the next three specimens, as well as adhesive failure between the adhesive and the adjacent part (instead of cohesive failure in the layer of the adhesive). This could be caused by the imperfect manual preparation of the bonded joint (variable thickness, air in the adhesive). Therefore, eight specimens were subjected to further research. The pull-up of the fibre was not found for these specimens during testing, only cohesive failure in the layer of the adhesive. The relationship between torque and rotation is shown in Fig. 17 for all eight specimens with appropriate mechanism of failure.
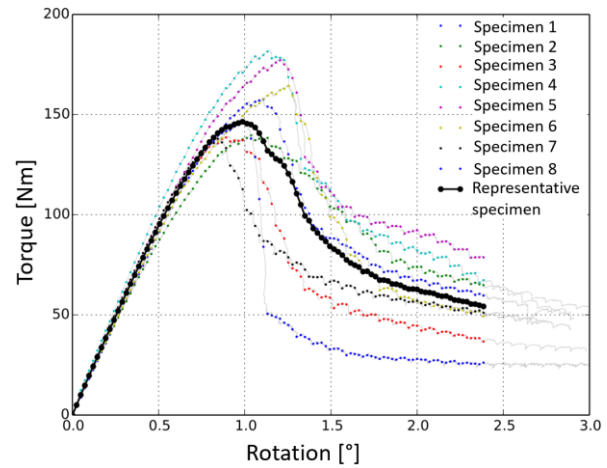

Figure 17. Comparison between tested specimens and the representative specimen

The results show the difference of the maximum torque value (about 25%) and the different stiffness of each specimen. After reaching the maximum torque value the degradation of the bonded joint occurs and the values of the torque vary by up to 70 %. This significant difference is caused by the different sizes of the active bonded surfaces. This, together with friction and broken glue (which still remains inside the joint), influences the value of the transmitted torque. The torque-rotation curve highlighted in Fig. 7 was considered to be a representative curve for the following optimisation. This curve was obtained by arithmetic average of all results. All the necessary parameters were found using the optimisation method and are shown in Tab. 6.

Parameters	Representative sample
k_n [GPa/m]	120
k_s [GPa/m]	130
k_t [GPa/m]	350
t_n [MPa]	2.3
t_s [MPa]	20.8
t_t [MPa]	14
G_{nc} [J/m^2]	141
G_{sc} [J/m^2]	3850
G_{tc} [J/m^2]	2850
α	1
r_g	0.903

Table 6. Cohesive, damage parameters and objective function

The parameters in the n and s directions were identified in previous research [Bernardin 2019] according to ASTM [ASTM D5528-13 2014, ASTM D7905M-14 2013]. Tab. 6 describes the cohesive and damage parameters of the representative specimen. The difference between torque and rotation of the experimentally obtained curves and the curves from FEM analysis is shown in Fig. 18.
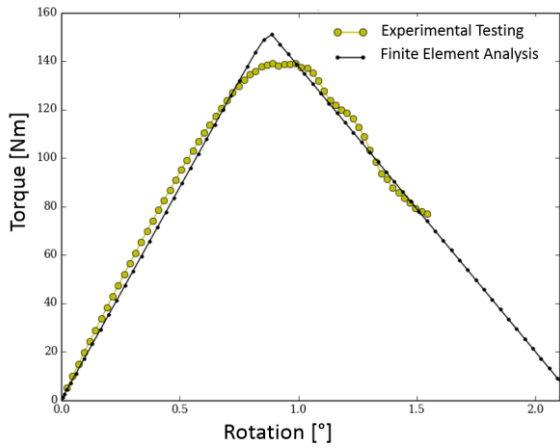
Figure 18. Relationship between torque and rotation of experimentally obtained curves and curves from FEM analysis

The participation of the failure mode i_a is based on 3D Power Law criterion and it is described by Eq. 8.

$$i_a = \frac{G_a}{G_{ac}} \cdot [100\ \%]\ , \qquad (8)$$

where a can be replaced by the specific mode (I, II or III). The participation of Mode I, II and III was determined using the results of FEM analysis and it is shown in Tab. 7.

	i_I - Mode I	i_{II} - Mode II	i_{III} - Mode III
Participation of mode [%]	$5 \cdot 10^{-5}$	$3 \cdot 10^{-4}$	99.99964

Table 7. The participation of failure modes in bonded joint

The predominance of Mode III was confirmed by the FEM results (the parameter i_{III} reaches almost 100%). According to the crack tip propagation detected in FEM, the parameters k_t, t_t, G_{tc} correspond to k_{III}, t_{III}, G_{IIIc} and have the biggest influence on the results. This corresponds to the real crack tip orientation and to the theory of the orthogonality of the pure mode orientation. The non-standardized samples do not have the same diameter along the length and contain sharp corners, notches, etc. It was also found that the stress distribution varies using different calculation methods (VCCT, CZM, Analytical calculation, XFEM) [Adams 1977, Aimmanee 2018, Kaya 1999, Chen 1992]. These are the main reasons that the shear stress propagation along the joint length (see Fig. 19) roughly, but not exactly, corresponds with the typical stress distribution in TLTL in general (see Fig. 3).
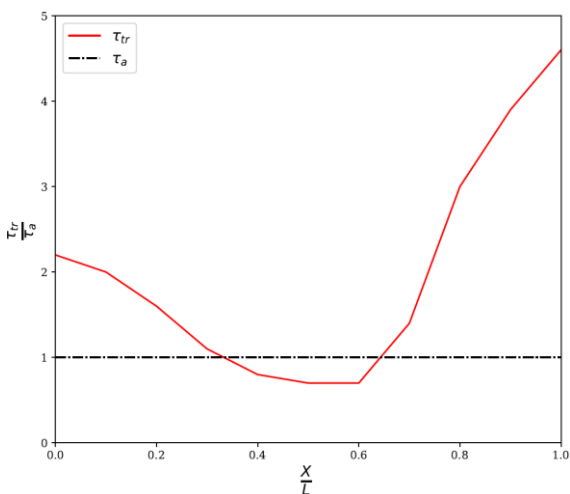

Figure 19. The stress distribution (τ_{tr}) and the idealised stress distribution (τ_a) in examined TLTL obtained by FEM in X direction

The following figures show the particular stress components in dependence on the Z direction (in plane shown in Fig. 15). Fig. 20 and Fig. 21 show the normal stresses σ_z and σ_x, Fig. 22 and Fig. 23 show the shear stresses in the XY and XZ planes τ_z and τ_y. All stresses were determined on the shorter side of the bonded surface, see $Z_{Section}$ (Fig. 15).
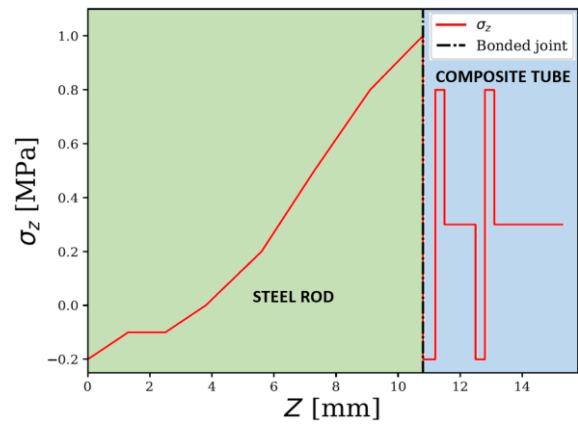

Figure 20. The normal stress σ_z in dependence on the Z direction obtained by FEM
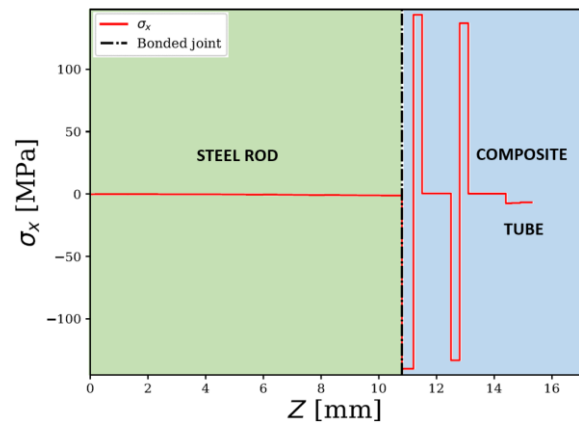

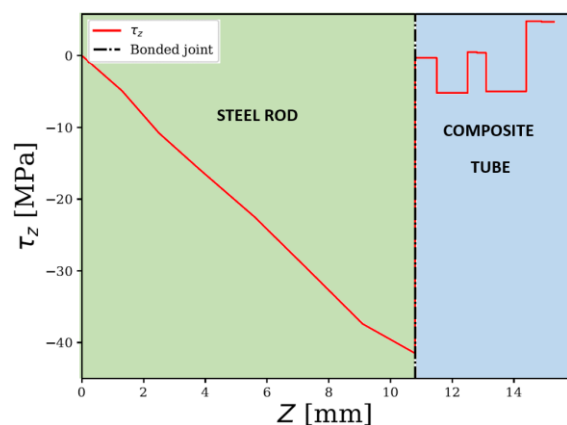**Figure 21.** The normal stress σ_x in dependence on the Z direction obtained by FEM

Figure 22. The shear stress in the XY plane τ_z in dependence on the Z direction obtained by FEM
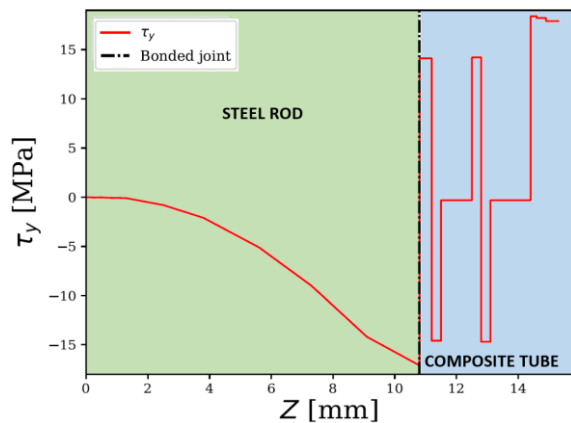
Figure 23. The shear stress in the XZ plane τ_y in dependence on the Z direction obtained by FEM

The CZM primarily evaluates the SERR values and not the stress values. Therefore, the previous stress comparison is for information only.

7 CONCLUSIONS

The mode ratio of TLTL was clarified using FEM analysis. Modes I and II were negligible, participation of Mode III was almost 100 %. Therefore, this work confirmed the suitability of the proposed method for identifying the cohesive and damage parameters of these joints related to Mode III. These parameters are suitable for a tubular lap joint under torsional loading, with similar surface roughness (Ra = 3.2 µm), for arbitrary adherend stiffness, arbitrary length and adhesive layer in a range from 0.05 mm to 0.4 mm, and for arbitrary material of adherends [Bernardin 2019, Sedláček 2005]. The parameters obtained for Mode I, II, and III can be used to predict the behaviour of any bonded joints loaded by pure modes (I, II, III) or by Mixed-mode loading. However, the biggest disadvantage of this method is the large dispersion of the experimental results. Therefore, this method does not yet seem to be a suitable option as a Mode III standard method. The statistical method was not used to evaluate the results due to the small number of samples. Performing the experimental measurement with a higher number of specimens (hundreds) and the use of statistical methods is needed to increase the accuracy of the results.

REFERENCES

[3M 1996] 3M, Scotch-Weld EPX Adhesive DP490. Created / Updated 1.11.1993 / 1.3.1996. Cited 27.11.2015, Available from https://www.shandhigson.co.uk/images/3M%20DP490.pdf.

[Adams 1977] Adams, R. D., et al. Stress Analysis of Adhesive Bonded Tubular Lap Joints. The Journal of Adhesion, 9(1), 1–18. (1977). DOI:10.1080/00218467708075095

[Aimmanee 2018] Aimmanee, S. A Unified Analysis of Adhesive-Bonded Cylindrical Coupler Joints, In Applied Adhesive Bonding in Science and Technology, InTech, 2018 DOI:10.5772/intechopen.72288

[ASTM D5528-13 2014] Standard Test Method for Determination of the Mode II Interlaminar Fracture Toughness of Unidirectional Fiber-Reinforced Polymer Matrix Composites, West Conshohocken, PA: ASTM International, 2014.

[ASTM D7905M-14 2013] Standard Test Method for Determination of the Mode II Interlaminar Fracture Toughness of Unidirectional Fiber-Reinforced Polymer Matrix Composites, West Conshohocken, PA: ASTM International, 2014.

[Barenblatt 1962] Barenblatt, G.I. Mathematical Theory of Equilibrium Cracks in Brittle, *Advances in Applied Mechanics 7*, 1962

[Belytschko 2009] Belytschko, T., et al. A review of extended/generalized finite element methods for material modeling. Modelling and Simulation in Materials Science and Engineering, 17(4), 43001. DOI:10.1088/0965-0393/17/4/043001

[Benzeggagh 1996] Benzeggagh, M. L., et al. Measurement of Mixed-Mode Delamination Fracture Toughness of Unidirectional Glass/Epoxy Composites with Mixed-Mode Bending Apparatus. Composites Science and Technology, Vol. 56, No. 4, 1996, DOI:10.1016/0266-3538(96)00005-X.

[Bernardin 2013] Bernardin, P. et al. Determination of the mechanical parameters of a bonded joint between a metal and a composite by comparing experiments with a finite-element model, Materiali in tehnologije, 47, 4(2013), pp. 417-421.

[Bernardin 2016] Bernardin, P. Thesis: Metal-to-composite joints. Pilsen, 2016

[Bernardin 2019] Bernardin, P. et al. Identification of the Cohesive Parameters for Modeling of Bonded Joints between Flat Composite Adherends, Tehnički vjesnik, XX, X(20xx), pp. XX-XX (In a review process)

[Camanho 2002] Camanho, P. P., et al. Mixed-Mode Decohesion Finite Elements for the Simulation of Delamination in Composite Materials. NASA/TM-2002-211737, NASA Langley Research Center, Virginia, USA, 2002.

[Chen 1992] Chen, D., et al. Torsional stress in tubular lap joints. International Journal of Solids and Structures, 29(7), 845–853. DOI:10.1016/0020-7683(92)90020-t

[Davidson 2010] Davidson B. Delamination Toughness Characterization of Laminated Composites, Encyclopedia of Aerospace Engineering, John Wiley & Sons, 2010, DOI:10.1002/9780470686652.eae181

[de Morais 2008] de Morais, A. B., et al. Mixed mode II + III interlaminar fracture of carbon/epoxy laminates, Compos Sci Technol, Vol. 68, No. 9, pp. 2022-2027, 2008.

[Ducept 2000] Ducept, F., et al. Mixed mode failure criteria for a glass/epoxy composite and an adhesively bonded composite/composite joint, *International Journal of Adhesion and Adhesives, Vol*. 20, No. 3 , pp. 233-244, 2000, DOI:10.1016/S0143-7496(99)00048-2

[Dudgale 1960] Dudgale, D.S. Yielding of Steel Sheets Containing Slits, *Journal of Mechanics and Physics of Solids, Vol*. 8, pp. 100-104, 1960

[Gay 2003] Gay, D., et al. Composite Materials - Design and Applications. Boca Raton, London, New York, Washington, D.C.: CRC Press LLC, 2003.

[Gliszczynski 2019] Gliszczynski, A., et al. Mode I Interlaminar Fracture of Glass/Epoxy Unidirectional Laminates. Part II: Numerical Analysis. Materials, 12(10), 1604. (2019) DOI:10.3390/ma12101604

[Griffith 1920] Griffith A. A. The Phenomena of Rupture and Flow in Solids. Philosophical Transactions, Series A, 221(1920), pp. 163-198.

[Inglis 1913] Inglis, C. E. Stresses in Plates Due to the Presence of Cracks and Sharp Corners, Transactions of the Institute of Naval Architects, 55 (1913), pp. 219-241.

[Irwin 1957] Irwin, G.R. Analysis of Stresses and Strains near the End of Crack Traversing a Plate. Journal of Applied Mechanics, 24 (1957), pp. 361-364.

[Kaya 1999] Kaya, A., et al. Three Dimensional Stress Analysis in Adhesively Bonded Joints with Rivets. Mathematical and Computational Applications, 4(3), 195–203. DOI:10.3390/mca4030195

[Krueger 2015] Krueger, R. The virtual crack closure technique for modeling interlaminar failure and delamination in advanced composite materials. In Numerical Modelling of Failure in Advanced Composite Materials (pp. 3–53). Elsevier. DOI:10.1016/b978-0-08-100332-9.00001-3

[Lašová 2017] Lašová, V. et al. Optimisation of metal-to-composite bonded joints with various adhesive layer configurations using finite element method, Technical gazette, Vol. 24, No. 5, 2017, pp. 1351-1354. DOI: 10.17559/TV-20160122124303

[Li 2009] Li, G. Cohesive Zone Model Based Analytical Solutions for Adhesively Bonded Pipe Joints under Torsional Loading, International Journal of Solids and Structures, Vol. 46, pp. 1205-1217, 2009

[Liao 1996] Liao, W.C., et al. The determination of Mode III fracture toughness in thick composite laminates, Composites Science and Technology, Vol. 56, No. 4, pp. 489-499, 1996.

[Mehrabadi 2013] Mehrabadi, F. A. Analysis of pure mode III and mixed mode (III + II) interlaminar crack growth in polymeric woven fabrics, Materials and Design, 44 (2013), pp. 429-437. DOI:10.1016/j.matdes.2012.07.071

[Ratcliffe 2004] Ratcliffe, J. G., et al. Characterization of the Edge Crack Torsion (ECT) Test for Mode III Fracture Toughness Measurement of Laminated Composites, Langley Research Center, Hampton, Virginia: NASA/TM-2004-213269, 2004.

[Reeder 2006] Reeder, J. R. 3D Mixed-Mode Delamination Fracture Criteria-An Experimentalist's Perspective, In: Proceedings of American Society for Composites, 21st annualtechnical conference, Dearborn, MI, United States, 2006.

[Sedláček 2005] Sedláček, R. Thesis: Design and experimental verification of new solutions of composite and metal parts in rotary drives of transport and agricultural machines. Prague, 2005

[Simulia 2019] Simulia. Abaqus Documentation 6.13. Dassault Systemes, Providence, RI, USA, 2013.

[Tahmasebi 1999] Tahmasebi, F.P. Finite Element Modeling of an Adhesive in a Bonded Joint. NASA Goggard Space Flight Center, 1992.

[Vigroux 2009] Vigroux, N. Thesis: Approximate methods for valuating mode mixity in delaminated composites. University of Florida, 2009

[Zemčík 2008] Zemčík, R., et. al. Numerical and experimental analyses of the delamination of cross-ply laminates, Materiali in tehnologije, 42, 4(2008), pp. 171-174.

CONTACTS:

Ing. Petr Bernardin, Ph.D.
University of West Bohemia, Regional Technological Institute, Faculty of Mechanical Engineering
Univerzitni 22, Pilsen, 306 14, Czech Republic
tel.: +420 377 63 8263, e-mail: berny@kks.zcu.cz

Ing. František Sedláček
University of West Bohemia, Regional Technological Institute, Faculty of Mechanical Engineering
Univerzitni 22, Pilsen, 306 14, Czech Republic
tel.: +420 377 63 8272, e-mail: fsedlace@kks.zcu.cz

prof. Ing. Václava Lašová, Ph.D.
University of West Bohemia, Regional Technological Institute, Faculty of Mechanical Engineering
Univerzitni 22, Pilsen, 306 14, Czech Republic
tel.: +420 377 63 8264, e-mail: lasova@kks.zcu.cz

Ing. Radek Kottner, Ph.D.
University of West Bohemia, European Centre of Excellence, New Technologies for Information Society, Faculty of Applied Sciences
Univerzitni 22, Pilsen, 306 14, Czech Republic
tel.: +420 377 63 2373, e-mail: kottner@kme.zcu.cz